scientific reports

OPEN

Crystal structures, phase transitions, thermodynamics, and molecular dynamics of organic–inorganic hybrid crystal [NH(CH₃)₃]₂ZnCl₄

A Young Kim[1], Changyub Na[1] & Ae Ran Lim[1,2✉]

Understanding the physical properties of organic–inorganic hybrid [NH(CH₃)₃]₂ZnCl₄ is necessary for its potential application in batteries and fuel cells due to its environmentally-friendly, and highly stable character. Here, we determine its overall properties in detail, such as its orthorhombic crystal structure, and phase transition temperatures associated with five different phases. Structural geometry was studied by the chemical shifts caused by the local field around ^1H. No changes were observed for the environment around ^1H for CH₃, whereas the ^1H chemical shifts around NH in the cation were shown due to the change in the hydrogen bond N−H···Cl. This is related to the change in Cl around Zn in the anion. In addition, the coordination geometry of ^{14}N and ^1H around ^{13}C exhibited increased symmetry at high temperatures. Finally, we were able to understand its molecular dynamics by the significant change with temperature observed from the spin–lattice relaxation time $T_{1\rho}$ values, which represent the energy transfer for the ^1H and ^{13}C atoms of the cation. The activation energies obtained from the $T_{1\rho}$ results were 3–4 times large at phase I (> 348 K) than at phase V and IV (< 286 K). The relaxations show that the energy barriers in phases IV and V are related to the reorientation of methyl groups around the triple symmetry axis, while the reorientation of methyl groups of the cation in phase I is related to as a whole.

Organic–inorganic hybrid compounds have been a field of great interest recently because of their potential applications. Their potential applications were mainly related to sensors, fuel cells, solar cells, light emitting transistor, and optical switches[1–5]. Recently, CH₃NH₃PbX_3 (X = Cl, Br, I) has been used for solar cells[6–8], but these materials were easily degraded in humid air and toxic due to the presence of Pb. Therefore, it is necessary to develop highly stable, eco-friendly hybrid perovskite solar cells. A new type of perovskite compound [(CH₃)₂NH₂] Zn(HCOOO)₃, consisting of a cation and a metal ion connected by formate ions, has been reported[9–12]. Especially, research on [NH₃(CH₂)$_n$NH₃]MX_4 (n=2, 3, 4, …, M represents divalent metals; Mn, Co, Cu, Zn, Cd, Pb, and X halogens; Cl, Br, I), with a focus on the physicochemical properties of their perovskite structure and dynamics investigation, has been garnering much attention[13–16]. As a new alternative, compounds of [NH(CH₃)₃]₂MX_4 may be described as sequences of alternating organic–inorganic layers[17–23]. For these organic-inorganic materials, the ammonium ion of the organic group forms the N−H···X hydrogen bond with the halide ion of the inorganic layer. The individual MX_4 tetrahedral anions in these materials were completely isolated and surrounded by organic [NH(CH₃)₃] cations. These substances were also expected to act as potential proton conductors owing to the existence of hydrogen bonds[24,25].

Solid-state nuclear magnetic resonance (NMR) provides information for studying local structure and mobility. By considering the temperature dependence of spin-lattice relaxation time of each nucleus, information can be obtained on the dynamical motion occurring in different environments[26–33]. Solid-state NMR on hybrid perovskite materials has also garnered considerable attention.

According to the previously reported, the phase transition temperatures T_C of [NH(CH₃)₃]₂ZnCl₄ crystal, trimethylammonium tetrachlorozincates, were reported by Kapustianik et al.[34] at 276.5 K and 310 K. According to Sveleba et al.[35], it was reported that the phase transition temperatures by dielectric properties occur at 269,

[1]Graduate School of Carbon Convergence Engineering, Jeonju University, Jeonju 55069, South Korea. [2]Department of Science Education, Jeonju University, Jeonju 55069, South Korea. ✉email: arlim@jj.ac.kr

282, and 309 K. After that, the T_C of $[NH(CH_3)_3]_2ZnCl_4$ defined by differential scanning calorimetry (DSC) has five phase transitions at 255 K, 282 K, 302 K, 320 K, and 346 K[19]. The $[NH(CH_3)_3]_2ZnCl_4$ crystal at 300 K has an orthorhombic structure with the space group *Pnma*, and its lattice constants are a=10.660 Å, b=9.629 Å, c=14.991 Å. The $[NH(CH_3)_3]_2ZnCl_4$ structure consists of trimethylammonium $[NH(CH_3)_3]$ cation and $[ZnCl_4]$ tetrahedron. This crystal is characterized by hydrogen bonds N−H···Cl connecting the organic cation to the inorganic anion. And, the ferroelectric properties and characterization of phase transitions were discussed by Raman spectroscopy[36].

In this study, the $[NH(CH_3)_3]_2ZnCl_4$ single crystals were grown using the aqueous solution method, and their structures, the phase transition temperatures, and thermal properties were investigated. Nuclear magnetic resonance (NMR) chemical shifts as a function of temperature were measured to investigate the coordination geometry for the ^1H and ^{13}C atoms in the cations of this crystal. From these results, the N−H···Cl hydrogen bond according to the ligands between the cations and anions was considered. And, the spin-lattice relaxation times $T_{1\rho}$ representing the energy transfer around the ^1H and ^{13}C atoms were discussed as a function of temperature, and their activation energies E_a are determined. The results of the single-crystal structure, NMR chemical shifts, and $T_{1\rho}$ are predicted important information on the crystal configuration and the energy transfer mechanism for the potential applications.

Methods
Crystal growth
Single crystals of $[NH(CH_3)_3]_2ZnCl_4$ were prepared from $[NH(CH_3)_3]Cl$ (Aldrich, 98%) and $ZnCl_2$ (Aldrich, 98%) in a ratio of 2:1. The mixed compounds were heated to make a homogeneous solution. The mixed solution was filtered once through filter paper, and colorless single crystals grown by slow evaporation were obtained after few days in a thermostat of 300 K.

Characterization
The lattice parameters of $[NH(CH_3)_3]_2ZnCl_4$ crystals were determined by single-crystal X-ray diffraction (SCXRD) at the Seoul Western Center of the Korea Basic Science Institute (KBSI). The crystal block was mounted on diffractometer (Bruker D8 Venture PHOTON III M14) equipped with a graphite-monochromated Mo-Kα (λ=0.71073 Å) radiation source. Data using SMART APEX3 and SAINT was collected and integrated. The structure was solved using direct methods and refined by full matrix least-squares on F2 using SHELXTL[37]. Additionally the powder XRD (PXRD) patterns of the $[NH(CH_3)_3]_2ZnCl_4$ crystals were measured using an XRD system with the same Mo-Kα used in SCXRD.

DSC measurement was performed using a DSC instrument (TA Instruments, DSC 25) with a heating speed of 10 °C/min between the 200 and 573 K temperature range under a flow of nitrogen gas. The changes of the single crystal according to temperature change were measured using an optical polarizing microscope. A hot stage was used to change the temperature (Linkam THMS 600).

Thermogravimetric analysis (TGA) was also measured with a heating speed of 10 °C/min in the temperature range between 300 and 873 K under nitrogen gas.

The magic angle spinning (MAS) NMR chemical shifts and the spin-lattice relaxation time $T_{1\rho}$ of the $[NH(CH_3)_3]_2ZnCl_4$ crystals were measured using a solid-state NMR spectrometer (Bruker, AVANCE III+) at the same facility, Western Seoul Center of the KBSI. The Larmor frequency for ^1H NMR experiment was 400.13 MHz, and that for the ^{13}C NMR experiment was 100.61 MHz. The sample was placed in cylindrical zirconia rotors and measured with a spin speed of 10 kHz for the MAS NMR measurements, in order to the reduce the spinning sideband. Chemical shifts were referenced to adamantane and tetramethylsilane (TMS) for ^1H and ^{13}C, respectively, as standard materials in order to accurate the chemical shift measurements. 1D NMR spectrum for ^1H and ^{13}C was performed in the delay time of 2–20 s. The ^1H $T_{1\rho}$ values were measured using π/2−τ spin-lock pulse for a duration of τ, and the π/2 pulse width was 3.65–4 μs. And, the ^{13}C $T_{1\rho}$ values were obtained by varying the duration of a ^{13}C spin-locking pulse after the CP preparation period. The ^{13}C $T_{1\rho}$ values were obtained using CP-τ acquisition.

Experimental results
FT-IR spectra
The FT-IR spectrum at 300 K was recorded within the 4000–500 cm^{-1} range. The result is shown in Fig. 1, and the peaks near 813 and 978 cm^{-1} are assigned to the N–C mode. And, the peak at 1253 cm^{-1} is related to the deformation vibration N–C–H. The bands observed 1410 and 1468 cm^{-1} are assigned to the CH_3 mode. The bands near 2769 and 3058 cm^{-1} are related to the stretching mode C–H, and the peak at 3493 cm^{-1} is the N–H stretching mode. This result agrees well the previously reported results of $[NH(CH_3)_3]_2CdCl_4$[23].

Crystal structure
Single crystal XRD results for the $[NH(CH_3)_3]_2ZnCl_4$ crystal grown here were obtained at 300 K. The single crystal structure has an orthorhombic system with space group *Pnma*, lattice constants a = 10.6279(4) Å, b = 9.6297(4) Å, c = 14.9880(7) Å, and Z = 4, which are consistent with previously reported results[19]. Figure 2 shows the thermal ellipsoid and atomic number for each atom, and XRD data of $[NH(CH_3)_3]_2ZnCl_4$ crystals are shown in Table 1. The infinite chains consisted of face-shared $ZnCl_4$ tetrahedra and four doubly bridging Cl$^-$ ions linked to adjacent Zn centers. As shown in Fig. 2, this compound is connected by three hydrogen bond N−H···Cl between the $[NH(CH_3)_3]$ cation and the $[ZnCl_4]$ anion. The bond-lengths for Zn−Cl, N−C, N−H···Cl and bond-angles for Cl−Zn−Cl and N−H···Cl are shown in Table 2. Here, the N−H···Cl hydrogen bond consists of an angle greater than 120°.
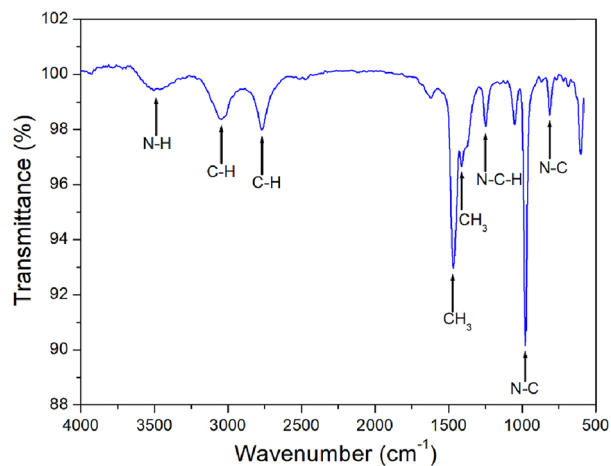
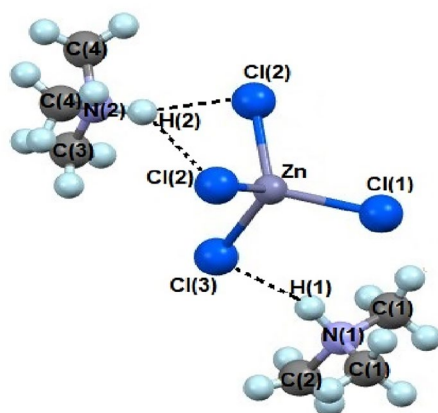**Figure 1.** FT-IR spectrum of $[NH(CH_3)_3]_2ZnCl_4$ at room temperature.

Figure 2. Crystal structure of $[NH(CH_3)_3]_2ZnCl_4$ at 300 K.

Chemical formula	$C_6H_{20}N_2ZnCl_4$
Weight	327.41
Crystal system	Orthorhombic
Space group	*Pnma*
T (K)	300
a (Å)	10.6279 (4)
b (Å)	9.6297 (4)
c (Å) α (°) β (°) γ (°)	14.9880 (7) 90 90 90
Z	4
V (Å³)	1533.92
Radiation type	Mo-Kα
Wavelength (Å)	0.71073
Reflections collected	12,566
Independent reflections	2009 ($R_{int} = 0.0333$)
Goodness-of-fit on F^2	1.037
Final *R* indices [I > 2sigma(I)]	$R_1 = 0.0485$, $wR_2 = 0.1355$
R indices (all data)	$R_1 = 0.0751$, $wR_2 = 0.1559$

Table 1. Crystal data and structure refinement for $[NH(CH_3)_3]_2ZnCl_4$ at 300 K.

Zn-Cl(1)	2.2510 (7)
Zn-Cl(2)	2.2577 (11)
Zn-Cl(2)#1	2.2577 (11)
Zn-Cl(3)	2.2855 (18)
N(1)-C(1)#1	1.433 (7)
N(1)-C(1)	1.433 (7)
N(1)-C(2)	1.471 (9)
N(2)-C(3)	1.377 (17)
N(2)-C(4)	1.442 (8)
N(2)-C(4)#1	1.442 (8)
N(1)-H(1)	0.9800
N(2)-H(2)	0.9800
C(1)-H(1)	0.9600
C(2)-H(2)	0.9600
C(3)-H(3)	0.9600
C(4)-H(4)	0.9600
N(1)-H(1)-Cl(3)	3.185
N(2)-H(2)-Cl(2)	3.627
N(2)-H(2)-Cl(2)#1	3.627
Cl(1)-Zn-Cl(2)	113.04 (5)
Cl(1)-Zn-Cl(2)#1	113.04 (5)
Cl(2)-Zn-Cl(2)#1	104.48 (7)
Cl(1)-Zn-Cl(3)	108.68 (7)
Cl(2)-Zn-Cl(3)	108.71 (5)
Cl(2)#1-Zn-Cl(3)	108.71 (5)
N(1)-H(1)-Cl(3)	160.96
N(2)-H(2)-Cl(2)	135.05

Table 2. Bond-lengths (Å) and bond-angles (°) for $[NH(CH_3)_3]_2ZnCl_4$ at 300 K.

Phase transition temperatures

The DSC thermogram for powder $[NH(CH_3)_3]_2ZnCl_4$ was measured in the temperature range from 200 to 573 K with the heating rate of 10 ℃/min. Figure 3 shows the four endothermic peaks at 257 K, 286 K, 326 K, and 348 K. And, the one strong endothermic peak at 553 K was obtained. The enthalpies for the five peaks were 2.54, 7.99, 7.53, 1.86, and 17.58 kJ/mol, respectively. Starting from 200 K, these five phases were denoted as phase V below 257 K, phase IV between 257 and 286 K, phase III between 286 and 326 K, phase II between 326 and 348 K, and phase I above 348 K, shown in Fig. 3.
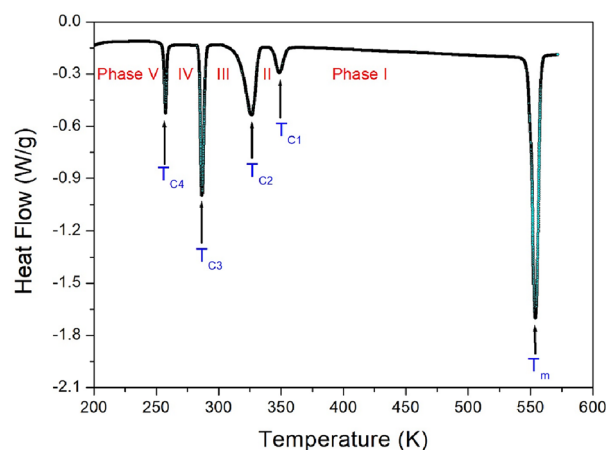

Figure 3. Differential scanning calorimetry curve of $[NH(CH_3)_3]_2ZnCl_4$ measured at a heating rate of 10 °C/min.

In order to know whether the five endothermic peaks shown in the DSC results shown in Fig. 3 are the phase transition temperatures or melting temperature, the changes of a single crystal were observed using an optical polarizing microscope with increasing temperature. Until the temperature rises to 530 K, the single crystal is almost unchanged, but the single crystal began to melt above 550 K.

In addition, a powder XRD experiment was measured according to the temperature change. The PXRD patterns in the range of 8°–50° (2θ) are shown at various temperature in Fig. 4. The PXRD patterns below 330 K (black) differ from that recorded above 330 K (red); this difference is related to the structural phase transition in T_{C2} (= 326 K). Furthermore, the XRD patterns recorded above 330 K differed from those recorded at 350 K (olive), and this difference is related to the phase transition in T_{C1} (= 348 K). These results are consistent with those of the DSC result. And, the theoretical XRD pattern at 300 K, which agrees well with the experimental pattern, is shown in Fig. 4.

The phase transition temperatures and melting temperature shown in the PXRD and polarizing microscope results are agree well with the endothermic peaks obtained in the DSC curve. From the DSC, PXRD, and optical polarizing microscopy results, the phase transition temperatures were determined as T_{C4} = 257 K, T_{C3} = 286 K, T_{C2} = 326 K, T_{C1} = 348 K, and the melting temperature was T_m = 553 K.

Thermal property

TGA curves shown in Fig. 5 were obtained with the increasing temperature. In the TGA curve, the partial decomposition temperature T_d representing a weight loss of 2 % was 495 K, and this material was thermal stable up to 495 K. The molecular weight of the $[NH(CH_3)_3]_2ZnCl_4$ crystal as the temperature increased was abruptly decreased by the partial decomposition. The molecular weight losses of 11 % and 22 % calculated from the total molecular weight were by the partial decomposition of HCl and 2HCl, respectively. The initial weight loss (45 %) was occurred in the range of 500–630 K. On the other hand, an endothermic peak at 342 K appeared in the
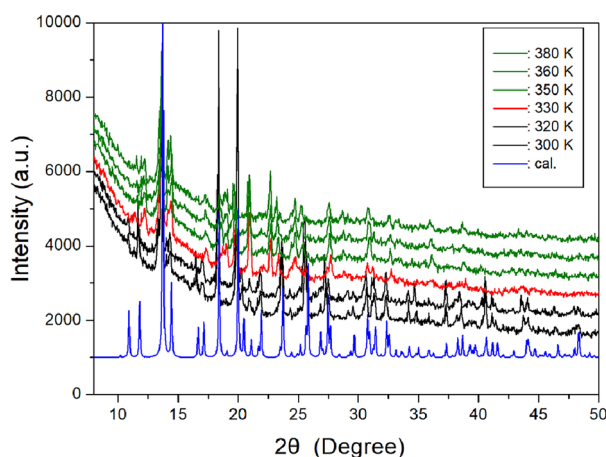

Figure 4. Powder X-ray diffraction patterns of $[NH(CH_3)_3]_2ZnCl_4$ at phases III, II, and I. The blue colour is the theoretical powder pattern at 300 K.
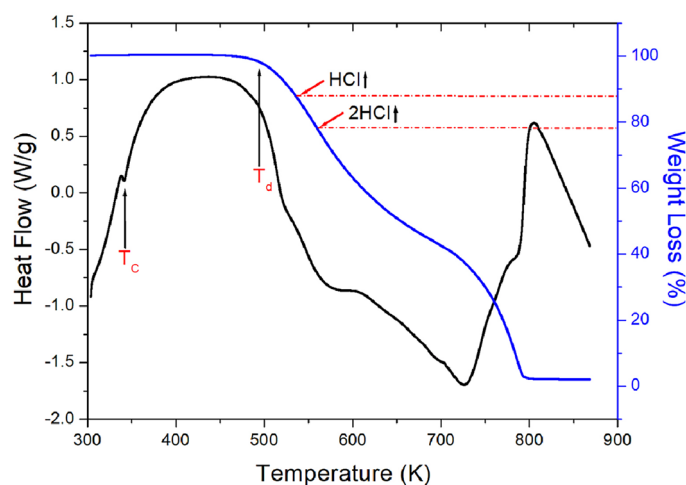

Figure 5. Thermogravimetric analysis and differential thermal analysis curves of $[NH(CH_3)_3]_2ZnCl_4$.

differential thermal analysis (DTA) curve, which is shown as a differential form of TGA, was in good agreement with the phase transition temperature T_{C1} shown in the DSC result. In addition, it was found that total weight loss occurred at temperatures near 800 K.

^{1}H and ^{13}C MAS NMR chemical shifts

The NMR chemical shifts for ^{1}H in the $[NH(CH_3)_3]_2ZnCl_4$ crystal were recorded at phases V, IV, III, II, and I, as shown in Fig. 6. The ^{1}H NMR spectra for NH and CH_3 were obtained, and their sidebands for ^{1}H spectrum were represented as the open circles and asterisks, respectively. At 300 K, the ^{1}H chemical shift for NH was recorded about 7.78 ppm and the ^{1}H chemical shift for CH_3 was obtained about 3.21 ppm. Depending on the temperature change, there is no change near T_{C4}, T_{C2}, and T_{C1}, but the ^{1}H chemical shift for NH near T_{C3} shows a change. As shown inside of Fig. 6, the ^{1}H chemical shifts for CH_3 were hardly change as the temperature increased, whereas the ^{1}H chemical shifts for NH were changed, and this result means that the coordination geometry around ^{1}H for CH_3 does not changes according to the temperature change, whereas the coordination geometry around ^{1}H for NH was changes.

The ^{13}C NMR chemical shifts of $[NH(CH_3)_3]_2ZnCl_4$ were measured in phases V, IV, III, II, and I with increasing temperature as shown in Fig. 7. In the structure of the crystal shown in Fig. 2, three ^{13}C atoms are bonded with ^{1}H and ^{14}N. The ^{13}C chemical shifts for CH_3 at 220 K of phase V showed three signals (46.98, 46.24, and 45.87 ppm), it reduced to two signals at 300 K of phase III (48.05 and 47.44 ppm), and it also reduced to one signal at 420 K of phase I (47.89 ppm). Although ^{14}N and ^{1}H are bonded around ^{13}C in the cation, the environments around ^{13}C can be different depending on the nearby Cl$^-$. That is, the change of ^{13}C chemical shifts was not seen near T_{C4}, whereas the change of chemical shift was large in T_{C3}. In addition, two signals were obtained between T_{C3} and T_{C2}, and at the temperature above T_{C1}, only one signal was obtained. The change in the number of ^{13}C chemical shifts can be explained as follows. That is, in phases V and IV, there are three CH_3 with different environments, and in phases III and II, there are two CH_3 with different environments. In particular, in phase I, it was found that all the environments around ^{13}C in CH_3 were the same. The number of peaks in the ^{13}C NMR spectra decreases with increasing temperature, indicating an increase in coordination symmetry around the $[NH(CH_3)_3]$ cations.

^{1}H and ^{13}C NMR spin-lattice relaxation times

To understand the spin-lattice relaxation time $T_{1\rho}$, the signal intensities of ^{1}H and ^{13}C NMR spectra were measured according to the change of the delay times. The decay curves by the change in the intensities and delay times are represented as following equation[38–40]:

$$P(t) = P(0)\exp(-t/T_{1\rho}), \tag{1}$$

where P(t) is the intensity of the spectrum at time t and P(0) is the intensity of the spectrum at time $t = 0$. The $T_{1\rho}$ values for ^{1}H and ^{13}C in $[NH(CH_3)_3]_2ZnCl_4$ are obtained using Eq. (1), and their results are represented in Fig. 8 at phases V, IV, III, II, and I. ^{1}H and ^{13}C $T_{1\rho}$ at phases V and IV increases as the temperature increases and show a maximum value near 300 K. The $T_{1\rho}$ values at phase I show a tendency to rapidly decrease again. The similar tendency of the two ^{1}H and ^{13}C $T_{1\rho}$ values means that ^{1}H and ^{14}N around ^{13}C are bonded, and ^{13}C and
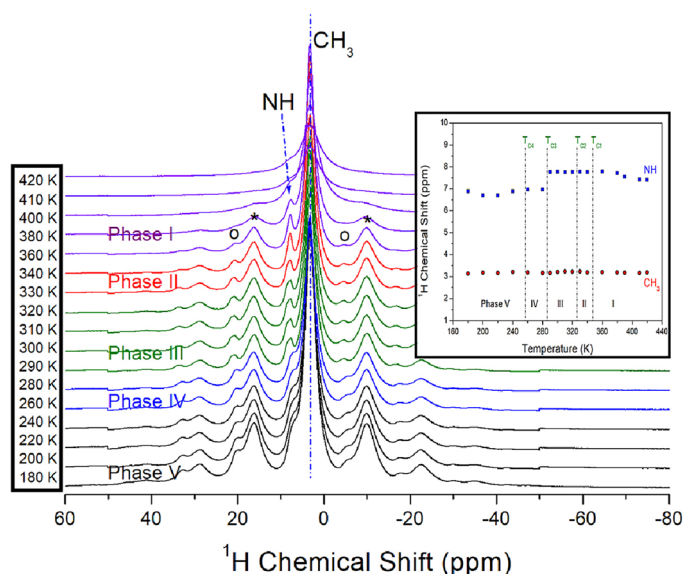

Figure 6. ^{1}H MAS NMR chemical shifts of NH and CH_3 in $[NH(CH_3)_3]_2ZnCl_4$ at phases V, IV, III, II, and I. The open circles are sideband for NH, and the asterisks are is sideband for CH_3 (inset: the ^{1}H chemical shifts for NH and CH_3 near phase transition temperatures).
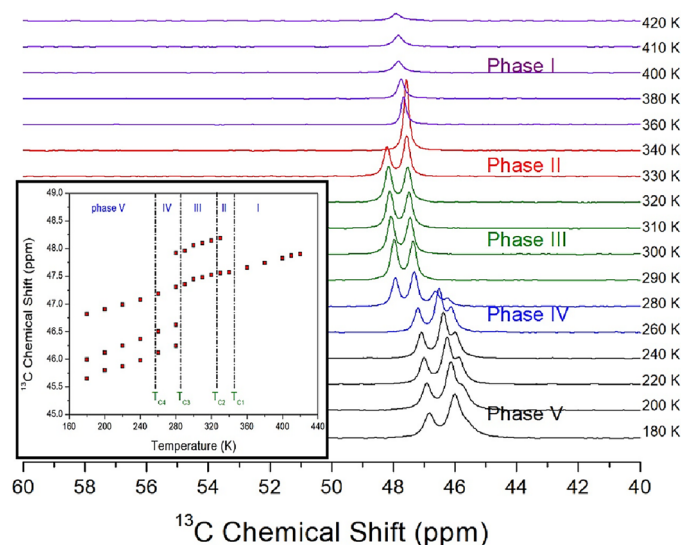
Figure 7. ^{13}C MAS NMR chemical shifts in $[NH(CH_3)_3]_2ZnCl_4$ at phases V, IV, III, II, and I (inset: the ^{13}C chemical shifts for CH_3 as a function of temperature).
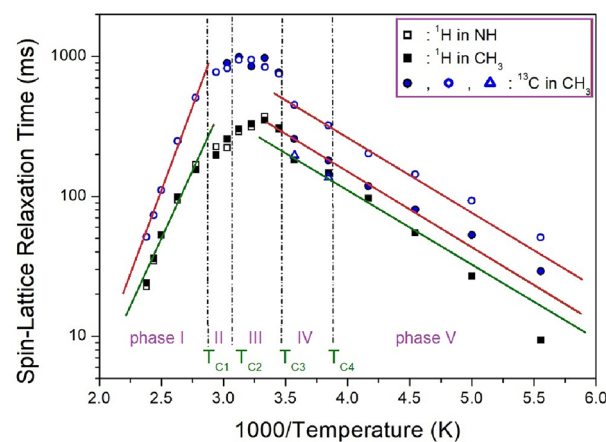

Figure 8. ^1H and ^{13}C NMR spin–lattice relaxation times $T_{1\rho}$ in $[NH(CH_3)_3]_2ZnCl_4$ at phases V, IV, III, II, and I. The slopes of lines are represented the activation energies by the $T_{1\rho}$ as a function of inverse temperature.

^{14}N around ^1H are bonded, so it is thought that they do the same motions. And, the fact that the ^{13}C $T_{1\rho}$ value is longer than the ^1H $T_{1\rho}$ value means that the energy transfer of ^1H bonded to the end of ^{13}C is easy. Near T_{C1}, T_{C2}, and T_{C4}, the $T_{1\rho}$ values for ^1H and ^{13}C are more or less continuous, but $T_{1\rho}$ values near T_{C3} are change discontinuous. To determine the magnitude of E_a depending the molecular dynamics, the logarithmic scale of $T_{1\rho}$ values vs. 1000/T are shown as the solid lines in Fig. 8; E_a for ^1H and was found to be 10.16 ± 0.88 kJ/mol at phases V and IV. And, the E_a for ^1H was 37.08 ± 2.21 kJ/mol at phase I. On the other hand, the E_a for ^{13}C obtained from the slope of $T_{1\rho}$ as the function of inverse temperature at phases V and IV was 9.80 ± 0.45 and 9.83 ± 0.42 kJ/mol, whereas it for ^{13}C was 45.04 ± 1.99 kJ/mol at phase I. Although the ^{13}C chemical shifts are slightly different, E_a at phases V and IV is almost the same within the error range. It is noteworthy that the differences in E_a at phases V, IV, and I are very large.

The ^1H and ^{13}C $T_{1\rho}$ values shows a tendency to increase rapidly at phases V and IV, whereas those shows decrease abruptly at phase I. The behaviours of the $T_{1\rho}$ for Arrhenius-type molecular motions are separate into fast- and slow-motion parts. Fast motion is expressed as $\omega_1\tau_C \ll 1$, $T_{1\rho}^{-1} \sim \exp(E_a/k_BT)$, and the slow motion as $\omega_1\tau_C \gg 1$, $T_{1\rho} \sim \omega_1^{-2} \exp(-E_a/k_BT)$[38]. At the boundary of 300 K, it is divided into fast and slow motion. The ^1H and ^{13}C $T_{1\rho}$ values at phases V and IV were in the fast-motion regime, whereas the ^1H and ^{13}C $T_{1\rho}$ values at phase I were attributed to the slow-motion regime.

Conclusion

Investigating of the growth, phase transition temperatures, and thermodynamics of the organic–inorganic hybrid $[NH(CH_3)_3]_2ZnCl_4$ crystals were considered. The orthorhombic structure of this crystal was determined by SCXRD, and the four phase transition temperatures of 257 K (= T_{C4}), 286 K (= T_{C3}), 326 K (= T_{C2}), and 348 K (= T_{C1}) were defined using DSC and PXRD results. The previously reported[19,34,35] phase transition temperatures may slightly differ depending on the crystal growth conditions. This crystal had the thermal stability of about 495 K, and weight loss resulting in the loss of the HCl and 2HCl moieties was observed with increasing temperature owing to thermal decomposition. From the chemical shifts caused by the local field around ^1H, the environments around ^1H for CH_3 does not changes according to the temperature change, whereas the environments around ^1H for NH was changes. And, the coordination geometry of ^{13}C becomes high symmetry as the temperature rises. As a result, the change in ^1H chemical shifts around NH in the cation is suggest be due to the change in the hydrogen bond N−H⋯Cl, which is related to the change in Cl around Zn in the anion. Finally, ^1H $T_{1\rho}$ and ^{13}C $T_{1\rho}$ values, which represent the energy transfer for the ^1H and ^{13}C atoms of the cation are changed significantly with temperature. The activation energies considered from the NMR $T_{1\rho}$ values for molecular motion were very high at high temperature of phase I than at phase V and IV. Additionally, based on the relaxation time $T_{1\rho}$ measurements in the rotational system for ^1H and ^{13}C at different temperatures, activation barriers for the molecular reorientation of the cation in phases I, IV, and V were determined. The activation energy barriers in phases IV and V are approximately four times lower than that in phase I. The relaxations show that in phases IV and V the energy barrier was related to the reorientation of methyl groups around the triple symmetry axis, and in phase I the reorientation of methyl groups of the cation was related to the entire rotation. This work provides an understanding of the fundamental properties for applications in organic–inorganic hybrid materials.

Data availability

The datasets generated and/or analysed during the current study are available in the CCDC 2321570.

References

1. Stranks, S. D. & Snaith, H. Metal-halide perovskites for photovoltaic and light-emitting devices. *J. Nat. Nanotechnol.* **10**, 391 (2015).
2. Hao, F., Stoumpos, C. C., Chang, R. P. H. & Kanatzidis, M. G. Anomalous band gap behavior in mixed Sn and Pb perovskites enables broadening of absorption spectrum in solar cells. *J. Am. Chem. Soc.* **136**, 8094 (2014).
3. Jeon, N. J. *et al.* Solvent engineering for high-performance inorganic–organic hybrid perovskite solar cells. I. *Nat. Mater.* **13**, 897 (2014).
4. Egger, D. A., Rappe, A. M. & Kronik, L. Hybrid organic–inorganic perovskites on the move. *Acc. Chem. Res.* **49**, 573 (2016).
5. Ye, H.-Y., Zhang, Y., Fu, D.-W. & Xiong, R.-G. An above-room-temperature ferroelectric organo-metal halide perovskite: (3-pyr-rolinium)(CdCl₃). *Angew. Chem. Int. Ed.* **53**, 11242 (2014).
6. Strelcov, E. *et al.* CH₃NH₃PbI₃ perovskites: Ferroelasticity revealed. *Sci. Adv.* **3**, e1602165 (2017).
7. Liu, Y. *et al.* Chemical nature of ferroelastic twin domains in CH₃NH₃PbI₃ perovskite. *Nat. Mater.* **17**, 1013 (2018).
8. Mauck, C. M. *et al.* Inorganic cage motion dominates excited-state dynamics in 2D-layered perovskites (CₓH₂ₓ₊₁NH₃)₂PbI₄ (x = 4–9). *J. Phys. Chem. C* **123**, 27904 (2019).
9. Asaji, T. & Ashitomi, K. Phase transition and cationic motion in a metal-organic perovskite, dimethylammonium zinc formate [(CH₃)₂NH₂][Zn(HCOO)₃]. *J. Phys. Chem.* **117**, 10185 (2013).
10. Abhyankar, N. *et al.* Understanding ferroelectricity in the Pb-free perovskite-like metal-organic framework [(CH₃)₂NH₂] Zn(HCOO)₃: Dielectric, 2D NMR, and theoretical studies. *J. Phys. Chem.* **121**, 6314 (2017).
11. Simenas, M. *et al.* Elucidation of dipolar dynamics and the nature of structural phases in the [(CH₃)₂NH₂][Zn(HCOO)₃] hybrid perovskite framework. *J. Mater. Chem. C* **7**, 6779 (2019).
12. Simenas, M. *et al.* Spectroscopic study of [(CH₃)₂NH₂][Zn(HCOO)₃] hybrid perovskite containing different nitrogen isotopes. *J. Phys. Chem.* **122**, 10284 (2018).
13. Mostafa, M. F. & El-khiyami, S. S. Crystal structure and electric properties of the organic–inorganic hybrid: [(CH₂)₆(NH₃)₂]ZnCl₄. *J. Solid State Chem.* **209**, 82 (2014).
14. Abdel-Adal, S. K., Kocher-Oberlehner, G., Ionov, A. & Mozhchil, R. N. Effect of organic chain length on structure, electronic composition, lattice potential energy, and optical properties of 2D hybrid perovskites [(NH₃)(CH₂)ₙ(NH₃)]CuCl₄, n = 2–9. *Appl. Phys. A* **123**, 531 (2017).
15. Staskiewicz, B., Czupinski, O. & Czapla, Z. On some spectroscopic properties of a layered 1,3-diammoniumpropylene tetrabro-mocadmate hybrid crystal. *J. Mol. Struct.* **1074**, 723 (2014).
16. Czapla, Z. *et al.* Structural phase transition in a perovskite-type NH₃(CH₂)₃NH₃CuCl₄ crystal—X-ray and optical studies. *Phase Trans.* **90**, 637 (2017).
17. Williams, I. D. & Brown, P. W. Structures of trimethylammonium tetrachlorometallates. *Acta Cryst.* **C48**, 259 (1992).
18. Ben Bechir, M., Karoui, K., Tabellout, M., Guidara, K. & Ben Rhaiem, A. Alternative current conduction mechanisms of organic-inorganic compound [N(CH₃)₃H]CuCl₄. *J. Appl. Phys.* **115**, 203712 (2014).
19. Ben Bechir, M., Karoui, K., Tabellout, M., Guidara, K. & Ben Rhaiem, A. Alternative current conduction mechanisms of organic-inorganic compound [N(CH₃)₃H]₂ZnCl₄. *J. Appl. Phys.* **115**, 153708 (2014).
20. Ben Bechir, M., Karoui, K., Tabellout, M., Guidara, K. & Ben Rhaiem, A. Electric and dielectric studies of the [N(CH₃)₃H]₂CuCl₄ compound at low temperature. *J. Alloys. Compd.* **588**, 551 (2014).
21. Ben Bechir, M. *et al.* [N(CH₃)₃H]₂ZnCl₄: Ferroelectric properties and characterization of phase transitions by Raman spectroscopy. *J. Appl. Phys.* **116**, 214104 (2014).
22. Karoui, K., Ben Bechir, M., Bulou, A., Guidara, K. & Ben Rhaiem, A. [N(CH₃)₃H]₂CuCl₄: Ab initio calculations and characteriza-tion of phase transitions by Raman spectroscopy. *J. Mol. Struct.* **114**, 161 (2016).
23. Ben Bechir, M. & Ben Rhaiem, A. Structural phase transition, vibrational analysis, ionic conductivity and conduction mechanism studies in an organic–inorganic hybrid crystal: [N(CH₃)₃H]₂CdCl₄. *J. Solid State Chem.* **296**, 122021 (2021).
24. Mostafa, M. F. & Hassen, A. Phase transition and electric properties of long chain Cd(II) layered perovskites. *Phase Trans.* **79**, 305 (2006).
25. Ionescu, D., Ciobanu, B. & Radinschi, I. Frequency resonant behaviour of the effective permittivity for a polyvalent liquid crystal in microwave range. *J. Optoelectron. Adv. Mater.* **9**, 2608 (2007).

26. Gedat, E. *et al.* Stray field gradient NMR reveals effects of hydrogen bonding on diffusion coefficients of pyridine in mesoporous silica. *Magn. Reson. Chem.* **39**, S149 (2001).
27. Vyalikh, A. *et al.* Evidence of microphase separation in controlled pore glasses. *Solid State Nucl. Magn. Reson.* **28**, 117 (2005).
28. Franssen, W. M. J. & Kentgens, A. P. M. Solid-state NMR of hybrid perovskites. *Solid State Nucl. Mag. Reson.* **100**, 36–44 (2019).
29. Milic, J. V. *et al.* Supramolecular engineering for formamidinium-based layered 2D perovskite solar cells: Structural complexity and dynamics revealed by solid-state NMR spectroscopy. *Adv. Energy Mater.* **9**, 1900284–1900296 (2019).
30. Lee, J., Lee, W., Kang, K., Lee, T. & Lee, S. K. Layer-by layer structural identifcation of 2D ruddlesden-popper hybrid lead iodide perovskites by solid-state NMR spectroscopy. *Chem. Mater.* **33**, 370–377 (2021).
31. Dahlman, C. J. *et al.* Dynamic motion of organic spacer cations in ruddlesden-popper lead perovskites probed by solid-state NMR spectroscopy. *Chem. Mater.* **33**, 642–656 (2021).
32. Shelyapina, M. G. *et al.* NMR study of intercalates and grafted organic derivatives of $H_2La_2Ti_3O_{10}$. *Molecules* **25**, 5229 (2020).
33. Dahlman, C. J. *et al.* Dynamic motion of organic spacer cations in Ruddlesden–Popper lead iodide perovskites probed by solid-state NMR spectroscopy. *Chem. Matter* **33**, 642 (2021).
34. Kapustianik, V. *et al.* Phase transitions in $(NH(CH_3)_3)_2ZnCl_4$ ferroelectric crystals. *Ferroelectrics* **192**, 121 (1997).
35. Sveleba, S. *et al.* Phase transitions in $[NH(CH_3)_3]_2MeCl_4$ (Me = Cd, Zn, Cu) crystals. *Phase Trans.* **46**, 245 (1994).
36. BenBechir, M. *et al.* $[N(CH_3)_3H]_2ZnCl_4$: Ferroelectric properties and characterization of phase transitions by Raman spectroscopy. *J. Appl. Phys.* **116**, 214104 (2014).
37. *SHELXTL v 6.10.* (Bruker AXS, Inc., 2000).
38. Abragam, A. *The Principles of Nuclear Magnetism* (Oxford University Press, 1961).
39. Harris, R. K. *Nuclear Magnetic Resonance Spectroscopy* (Pitman, 1983).
40. Koenig, J. L. *Spectroscopy of Polymers* (Elsevier, 1999).

Acknowledgements

Author contributions

A.R.Lim designed the project, NMR experiment, and wrote the manuscript. A.Y.Kim performed IR, DSC, and TGA experiments. C.Na performed X-ray experiment.

Competing interests

The authors declare no competing interests.

Additional information

Correspondence and requests for materials should be addressed to A.R.L.

Reprints and permissions information is available at www.nature.com/reprints.

Publisher's note Springer Nature remains neutral with regard to jurisdictional claims in published maps and institutional affiliations.